

Hongli Ji¹

State Key Laboratory of Mechanics and Control of
Mechanical Structures,
Nanjing University of Aeronautics and
Astronautics,
Yudao Street 29,
Nanjing 210016, China
e-mail: jihongli@nuaa.edu.cn

Xiaoning Zhao

State Key Laboratory of Mechanics and Control of
Mechanical Structures,
Nanjing University of Aeronautics and
Astronautics,
Yudao Street 29,
Nanjing 210016, China
e-mail: zxning16@nuaa.edu.cn

Ning Wang

State Key Laboratory of Mechanics and Control of
Mechanical Structures,
Nanjing University of Aeronautics and
Astronautics,
Yudao Street 29,
Nanjing 210016, China
e-mail: wangning96@nuaa.edu.cn

Wei Huang

School of Mechanical Engineering,
Nanjing University of Science and Technology,
Xiaolingwei 200,
Nanjing 210094, China
e-mail: huangwei91@njtu.edu.cn

Jinhao Qiu

State Key Laboratory of Mechanics and Control of
Mechanical Structures,
Nanjing University of Aeronautics and
Astronautics,
Yudao Street 29,
Nanjing 210016, China
e-mail: qiu@nuaa.edu.cn

Li Cheng

Department of Mechanical Engineering,
Hong Kong Polytechnic University,
Hung Hom,
Kowloon 999077, Hong Kong, China
e-mail: li.cheng@polyu.edu.hk

A Circular Eccentric Vibration Absorber With Circumferentially Graded Acoustic Black Hole Features

A previously proposed planar axisymmetric dynamic vibration absorber (DVA), with embedded acoustic black hole (ABH) features, has been shown to suffer from the very selective coupling with the host structure, thus compromising its vibration reduction performance. To tackle the problem, an eccentric ABH-based circular DVA whose thickness profile is tailored according to a circumferential gradient variation is proposed. This new configuration preserves the ABH profile in the radial direction and breaks the axisymmetric of the original DVA design at the same time. While the former permits the ABH features to fully play out in a continuous manner, the later entails a more effective coupling with the host structure. These salient properties have been demonstrated and confirmed both numerically and experimentally by examining a benchmark plate structure. For analyses, a coupling model embracing the host structure and the add-on DVAs is established which allows the calculation of the coupling coefficient, a vital quantity to guide the DVA design. Studies demonstrate the advantages of the proposed DVA over existing designs for the same given mass. The enriched structural coupling and the enhanced modal damping, arising from the eccentric and circumferentially graded ABH design, are shown to be the origin of such improvement. All in all, the physical process underpinning the dynamic absorber principle and waveguide absorber from the host structures is simultaneously consolidated, thus leading to superior broadband structural vibration suppression. [DOI: 10.1115/1.4053475]

Keywords: acoustic black hole, vibration control, dynamic vibration absorber, coupling analysis, dynamics, modal analysis, structural dynamics and control

1 Introduction

Structural vibration is a vital problem in transportation vehicles such as aircraft, high-speed trains and cars, etc., due to the use of light-weight materials and structures [1,2]. As a passive damping technique, acoustic black hole (ABH) structures have been drawing an increasing attention because of their easy-to-realize and broadband wave focusing and energy dissipation properties. In one-dimensional cases, the thickness of an ABH wedge is

tailored according to a power-law variation [3]. As a result, the phase velocity of the flexural waves gradually reduces to zero when approaching the tapered edge, thus resulting in zero wave reflection theoretically. Similar phenomena can also be realized in two-dimensional cases to form a type of lens which can trap the wave energy to a specific location [4]. Through such tailoring and employing a small amount of damping materials within the thinnest part of the ABH region, flexural waves can be efficiently slowed down, focalized, and eventually dissipated. The entire process is conducive to promising engineering applications in addition to vibration suppressions of structures.

Extensive research on ABHs has been reported at an accelerating pace during the last decade. Existing works involve multiple aspects ranging from theoretical analyses [3–8], experimental investigations [9–12], structural design [13–17] and optimization [18–20]

¹Corresponding author.

Contributed by the Technical Committee on Vibration and Sound of ASME for publication in the JOURNAL OF VIBRATION AND ACOUSTICS. Manuscript received September 8, 2021; final manuscript received December 27, 2021; published online February 7, 2022. Assoc. Editor: Mostafa Nouh.

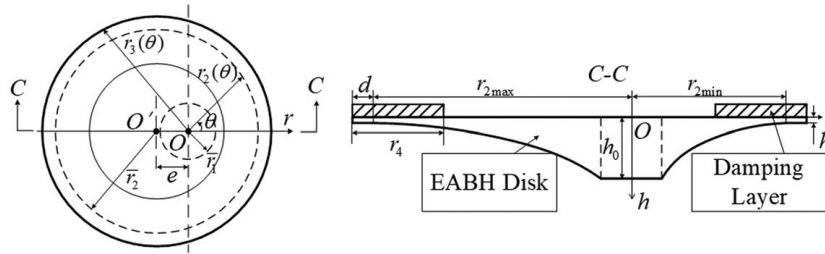


Fig. 1 Schematic of a 2D asymmetric EABH-DVA

as well as some emerging engineering applications such as vibration and noise reduction and energy harvesting [21–25]. Pelat et al. [26] and Zhao et al. [27] gave detailed and comprehensive reviews of the state-of-the-art on ABH research and some potential applications. In most of the above studies, ABHs are embedded into a structure. However, the appealing lightweight nature of ABH structures, as a result of thickness thinning and material removal, is also accompanied by some adverse effects on their compromised static properties such as reduced stiffness and strength, which is detrimental when used as load-bearing components.

Dynamic vibration absorber (DVA), as a kind of add-on vibration reduction devices, is widely used to suppress undesirable vibrations of a structure [28]. The basic form of a DVA contains a mass component connected by spring and damping elements to the host structure. Through a precise tuning of the DVA parameters, the vibration response of the host structure can be significantly reduced at the tuning frequency owing to its strong interaction with the DVA. However, traditional dynamic absorbers are usually used for single-mode suppression because they can only match a single frequency of the host structure or mechanical system [29]. To achieve better performance, various studies have been conducted involving different damping models [30–32], multi degree-of-freedom systems [33–35], and continuous systems [36,37]. In addition, optimal design of DVA has also been addressed [38,39]. Despite the existing efforts, the design of more robust, efficient, and simple DVAs is still needed to cope with practical and broadband vibration control applications.

Recently, the idea of designing add-on ABH-based dynamic dampers was proposed for the broadband vibration suppressions [40]. The working principle embraces the advantages of both dynamic vibration absorbers and waveguide absorbers [40–42]. Early adoption of ABH principle in a DVA structure is a 1D resonant beam damper proposed by Zhou et al. [40], followed by more complex designs such as an ABH-based circular dynamic vibration absorber by Ji et al. [41] and a planar swirl-shaped ABH absorber by Zhou et al. [42]. It is worth mentioning that the two-dimensional ABH-based dynamic vibration absorber (2D ABH-DVA), proposed by Ji et al. [41], was designed to cope with multi-directional flexural waves. However, taking the form of a circular disc, the 2D ABH-DVA shows obvious deficiencies. In fact, due to its axisymmetric geometry, only a few modes of the 2D ABH-DVA can be coupled with the host structure despite the abundant modes and the rich dynamic existing in the structure. A coupling analysis indicated that only the circumferential zeroth- and first-order modes of the 2D ABH-DVA can possibly be coupled with the host structure. This selective coupling pattern hinders the ultimate vibration suppression ability of the device.

To tackle the aforementioned problem, the present study proposes a new eccentric circular ABH-DVA (abbreviated as EABH-DVA), which features typical ABH thickness profile in the radial direction alongside a continuously graded thickness variation along the circumferential direction. The targeted outcome is a compact and light-weight device with enriched ABH features and enhanced coupling with a host structure onto which it is surface-mounted to achieve broadband vibration suppressions without a complex tuning procedure. It is shown that the new

structure not only preserves the basic ABH features in terms of dynamics and damping but also enriches the number of modes that can be coupled with the host structure, all owing to the breaking of the symmetry in the eccentric circular DVA arising from the circumferentially graded thickness variation. For analyses, a coupling coefficient is defined to quantify the coupling between the 2D ABH-DVA and the host structure. Its mathematical expression, allowing for subsequent numerical calculation and analyses, is derived, which is applicable for any complex structures. Finite element (FE) analyses are conducted with comparisons made with other existing DVA designs on the basis of equal allowable added mass. The superior vibration suppression performance of the proposed 2D ABH-DVA is demonstrated and finally verified by experiments.

2 EABH-DVA Design and Simulation Model

2.1 Geometry of the EABH-DVA. The proposed 2D EABH-DVA is shown in Fig. 1. It contains three domains: a uniform central plateau to be attached to a host structure later on, an annular domain of varying thickness and an annular domain of uniform thickness, defined by three concentric circles with radii, \bar{r}_1 , \bar{r}_2 , and \bar{r}_3 , respectively. Note the two outer circles of radii \bar{r}_2 and \bar{r}_3 are eccentric with respect to the central plateau with a thickness h_0 , where O is the center of the central plateau and O' is the center of the two outer circles. The distance, e , between O and O' , is the eccentricity. Taking O as the origin of the polar coordinate system as shown in Fig. 1, the radii of the two outer circles are mathematically governed by

$$r_2(\theta) = -e \cos \theta + \sqrt{\bar{r}_2^2 - e^2 \sin^2 \theta} \quad (1)$$

$$r_3(\theta) = -e \cos \theta + \sqrt{(\bar{r}_2 + d)^2 - e^2 \sin^2 \theta} \quad (2)$$

The maximum and minimum values of r_2 are $r_{2\max} = r_2(\pi) = \bar{r}_2 + e$ at $\theta = \pi$ and $r_{2\min} = r_2(0) = \bar{r}_2 - e$ at $\theta = 0$, respectively. There exists $\bar{r}_3 = \bar{r}_2 + d$, in which d is the width of the outer uniform domain.

The annular domain of varying thickness in the EABH-DVA is defined by $\bar{r}_1 \leq r \leq r_2(\theta)$. It is assumed that the thickness variation along the radial direction corresponding to a given θ satisfies a power law relationship, changing from h_0 at \bar{r}_1 to h_1 at $r_2(\theta)$. Therefore, the thickness variation can be described by

$$h(r) = \begin{cases} h_0, & (0 \leq r \leq \bar{r}_1) \\ \varepsilon |r - r_2(\theta)|^m + h_1, & (\bar{r}_1 \leq r \leq r_2(\theta)) \\ h_1, & (r_2(\theta) \leq r \leq r_3(\theta)) \end{cases} \quad (3)$$

and

$$\varepsilon(\theta) = \frac{h_0 - h_1}{|\bar{r}_1 - r_2(\theta)|^m} \quad (4)$$

It can be seen that the circular EABH-DVA disk follows a continuous thickness profile variation in both radial and circumferential

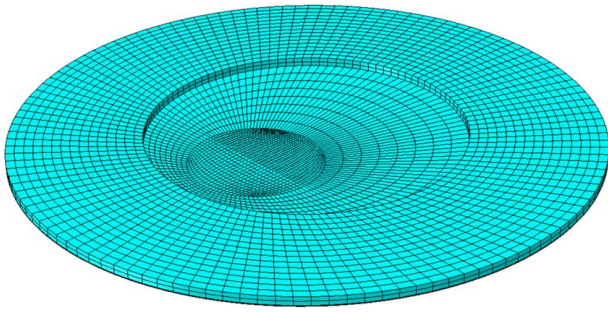


Fig. 2 Finite element model of the EABH-DVA

directions. While the thickness variation in the radial direction follows the standard ABH thickness profile (power-law), the variation along the circumferential is continuous with a gradient. An annular damping layer with a constant thickness h_d and a width r_d is bonded along the outer edge of the disk, as shown in Fig. 1. The whole design is intended to improve the performance of device while preserving the essential ABH features.

2.2 Wave Energy Focalization in the EABH-Disk. In order to verify the ABH-specific features in the EABH disk, FE simulations are first conducted to investigate the wave propagation characteristics in the EABH disk without damping layer. Geometrical parameters of the EABH disk are tabulated in Table 2. A typical ABH curve $m=2$ is selected. The model is discretized and assembled using 3D solid elements (C3D20R). To guarantee the simulation accuracy, a minimum of ten elements per wavelength was used. The FE meshing of the EABH-DVA is shown in Fig. 2. An incident wave, namely a five-cycle burst tone with a central frequency 20 kHz, is applied at the central plateau as shown in Fig. 3.

The out-of-plane displacement response at different time instants is given in Fig. 4, showing the wave propagation process in the EABH disk. The incoming flexural waves are indeed compressed and focused around the outer edge of the device due to the continuously diminishing thickness in the radial direction, similar to the wave focalization characters in typical one-dimensional ABH wedges. This creates typical wave trapping effect that would better promote structural loss when proper damping is added at a later stage. This is also conducive to the widening of the vibration reduction band, which will be discussed in the later sections. Furthermore, the asymmetric feature of the EABH disk induces uneven distributions of wave energy in the circumferential direction as shown in Fig. 4, also conducive to creating enriched multimodal

coupling with the host structure, which will be further investigated in Sec. 3.3.

2.3 Simulation Model of the EABH-DVA and Host Structure.

The EABH-DVA is to be attached to a host structure, exemplified by a rectangular plate, using either glue or a bolt, as shown in Fig. 5(a). Since it is an add-on device, rather than an embedded indentation into the host structure, its inclusion does not jeopardize the stiffness or the mechanical strength of the host structure. For comparisons, two more conventional absorbers: a symmetrical ABH-DVA (SABH-DVA) and an eccentric uniform DVA of equal mass (EEM-DVA), as shown in Fig. 6, are also examined. The geometry of the SABH-DVA is generated by setting the eccentricity e to 0. The EEM-DVA has its diameter equal to \bar{r}_3 with a uniform thickness, the value of which is determined according to the equal mass rule.

The total mass of the EABH-DVA is 0.0671 kg, which is 5.74% of the host structure. All three types of DVAs contain the same amount of damping materials in the form of an annular layer bonded onto the devices as shown in Fig. 6. Both the host structure and the ABH discs are made of aluminum, and the damping material is butyl rubber. The dimension of the host plate measures $l_a \times l_b \times l_c$, that is, 300 mm \times 240 mm \times 6 mm in the present case. Placing the origin of the coordinate system at the center of the plate a transverse excitation force of 1 N in amplitude is applied at (100, 50) mm over the plate. The EABH-DVA is rigidly connected to the host structure at (-120, -90) mm, and at 45-degree angle with respect to the plate's horizontal lower edge, as shown in Fig. 5(b). It should be noted that the optimization of installation location is not considered here. A location near one of the corners of the plate was chosen because the corners of a plate with free boundaries would undergo large vibration for nearly all modes. We hope that, even in the absence of meticulous choice of the installation location, the ABH-DVA can still couple with as many modes as possible in a given and broad frequency range. The material and geometrical parameters of the host structure and those of the three absorbers are listed in Tables 1 and 2, respectively.

Numerical simulations are first carried out to understand the dynamics of the host structure, each of the three add-on devices and the corresponding combined systems using ABAQUS. Shell elements are used for the host structure and 3D solid elements (C3D20R) for the add-on structures. To guarantee the accuracy of the numerical simulation, refined grids are used near the outer edges of the EABH-DVA and SABH-DVA, and the mesh size is set to ensure at least ten elements per wavelength. For modal analyses, free boundary condition is used for both host structure and the three combined systems and clamped boundary condition is

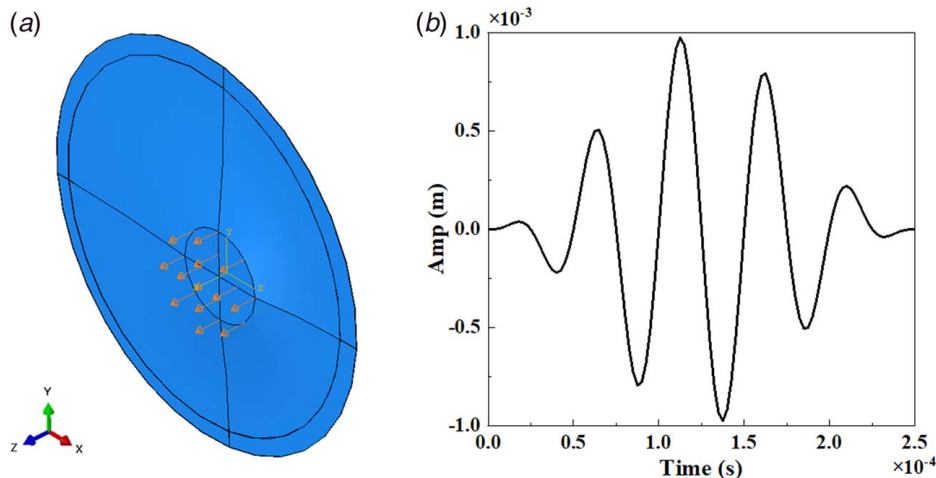


Fig. 3 FE simulation of wave propagation in an EABH: (a) FE model and (b) excitation signal

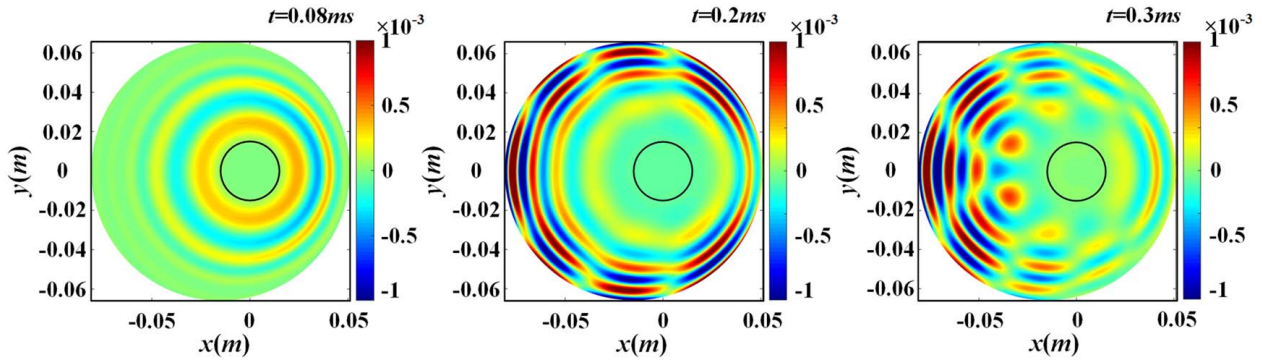


Fig. 4 Out-of-plane displacement response versus time subject to a tone-burst wave input

imposed over the installation interface (the central plateau) of the add-on structures. Clamped boundary condition for the add-on structures will simplify the formulation of the coupling analysis to be discussed later.

3 Coupling Analyses

3.1 Dynamic Coupling Between the Host Structure and the Add-On Device. The discretized dynamic equation for each subsystem (add-on device and the host structure) can be encapsulated in the following discretized form:

$$\mathbf{M}_s \ddot{\mathbf{w}}_s + \mathbf{C}_s \dot{\mathbf{w}}_s + \mathbf{K}_s \mathbf{w}_s = \mathbf{F} \quad (5)$$

$$\mathbf{M}_A \ddot{\mathbf{w}}_A + \mathbf{C}_A \dot{\mathbf{w}}_A + \mathbf{K}_A \mathbf{w}_A = 0 \quad (6)$$

where \mathbf{M}_s , \mathbf{C}_s , and \mathbf{K}_s are the mass, damping, and stiffness matrices for the host structure, respectively, and \mathbf{M}_A , \mathbf{C}_A , and \mathbf{K}_A are those

for the add-on structure; \mathbf{w}_s and \mathbf{w}_A are their corresponding nodal displacements, respectively; and \mathbf{F} is the excitation force on the host structure. Obviously, the out-of-plane motion, in both the host structure and the add-on devices, dominates the vibration as well as the main source of damping.

Using the modal superposition method after modal mass normalization, Eqs. (5) and (6) can be cast into the following form in the principal modal coordinate system as:

$$\mathbf{I} \dot{\mathbf{q}}_s + [2\omega_s \zeta_s] \dot{\mathbf{q}}_s + [\omega_s^2] \mathbf{q}_s = \mathbf{F}_m \quad (7)$$

$$\mathbf{I} \dot{\mathbf{q}}_A + [2\omega_A \zeta_A] \dot{\mathbf{q}}_A + [\omega_A^2] \mathbf{q}_A = 0 \quad (8)$$

where \mathbf{q}_s is the modal coordinates of the host structure; \mathbf{I} is a unit matrix; $[2\omega_s \zeta_s]$ is a diagonal matrix with its i th diagonal element equal to $2\omega_{si} \zeta_s$ with ω_{si} and ζ_s being the natural frequencies and the corresponding modal damping ratios of the plate. $[\omega_s^2]$ is another diagonal matrix containing only non-zero ω_{si}^2 as diagonal elements. Replacing sub-index s by A , all quantities apply to the absorber.

Since the interfacial area between the host structure and the add-on structure is small with respect to the bending wavelength, it is assumed that the motion on the interface is solely determined by the displacement of the node at the center of the interface. For nodal number n , the out-of-plane displacement component, w_{sn} , and the rotational angles, θ_{nx} and θ_{ny} , are as follows:

$$w_{sn} = \mathbf{G}_1 \Phi_s \mathbf{q}_s \quad (9)$$

$$\theta_{nx} = \mathbf{G}_2 \Phi_s \mathbf{q}_s \quad (10)$$

$$\theta_{ny} = \mathbf{G}_3 \Phi_s \mathbf{q}_s \quad (11)$$

where Φ_s is the modal matrix of the host structure, and the \mathbf{G}_k ($k = 1, 2, 3$) are vectors of dimension $1 \times 6N_s$ with all elements equal to 0 except that the $[6(n-1) + k + 2]$ th element equals 1, as

$$\mathbf{G}_k = \{ 0 \dots 0, 1, 0 \dots 0 \} \quad (12)$$

$[6(n-1) + k + 2]$ th element is 1.

where N_s is the number of FE nodes of the host structure.

For simplicity, the equations have been restructured so that only the out-of-plane displacement and the two rotational angles with respect to x and y axes are considered in each node of the host structure and only the out-of-plane displacement is considered in the add-on structure.

With the add-on structure attached to the n th node of the host structure, the displacement of the add-on device can be expressed as follows:

$$\mathbf{w}_A = \Phi_A \mathbf{q}_A + \{1\} w_{sn} + \mathbf{R}_y \theta_{nx} + \mathbf{R}_x \theta_{ny} \quad (13)$$

where Φ_A is the modal matrix of the add-on structure and \mathbf{q}_A is its modal coordinates, w_{sn} , θ_{nx} , and θ_{ny} are defined in Eqs. (9)–(11),

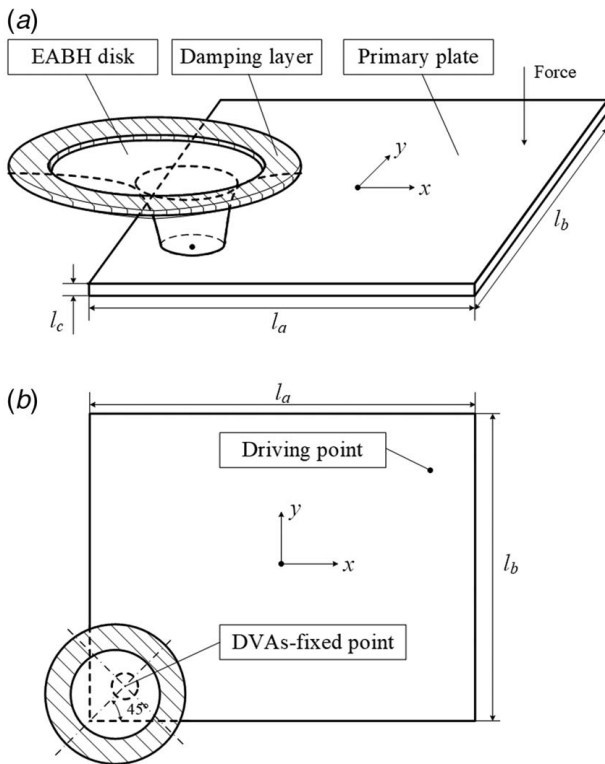


Fig. 5 Synthesis system: (a) 3D view and (b) vertical view

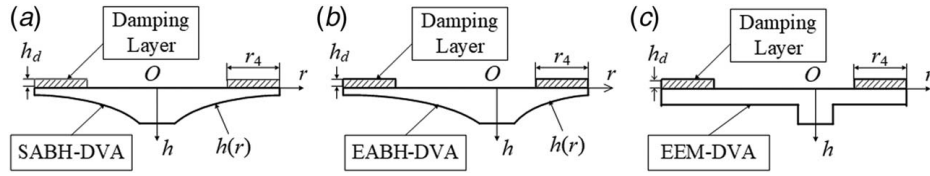


Fig. 6 Different add-on structures: (a) SABH-DVA, (b) EABH-DVA, and (c) EEM-DVA

Table 1 Material parameters

	Aluminum	Damping material
Young's modulus (MPa)	70000	200
Poisson's ratio	0.346	0.45
Density (kg/m ³)	2710	1850
Material loss factor	0.001	0.1

Table 2 Structural and geometric parameters

Parameters	EABH-DVA	ABH-DVA	EEM-DVA
m	2	2	/
ε	$2.8/(r_2(\theta) - \bar{r}_1)^2$	0.00138	/
r_1/mm	15	15	15
\bar{r}_2/mm	60	60	60
$r_{2\text{max}}/\text{mm}$	75	60	75
$r_{2\text{min}}/\text{mm}$	45	60	45
e/mm	15	0	15
d/mm	6	6	6
h_0/mm	3	3	3
h_1/mm	0.2	0.2	0.73
h_d/mm	2	2	2
r_4/mm	30	30	30

$\{1\}$ is a vector of $N_A \times 1$ with all the components equal to 1, \mathbf{R}_y is a vector of $N_A \times 1$ with each component equal to the y coordinate of the corresponding node, and \mathbf{R}_x is a vector of $N_A \times 1$ containing the x coordinate of the corresponding node. Obviously, $\{1\}$, \mathbf{R}_y , and \mathbf{R}_x are the modal vectors of the three rigid modes. According to Eq. (13), the displacement of the add-on structure includes its elastic vibration and the three rigid modes.

Substitution of Eq. (13) into Eq. (6) and utilization of Eqs. (7) and (8) give

$$\mathbf{I}\ddot{\mathbf{q}}_A + \Phi_A^T \mathbf{M}_A (\{1\} \mathbf{G}_1 + \mathbf{R}_y \mathbf{G}_2 + \mathbf{R}_x \mathbf{G}_3) \Phi_s \dot{\mathbf{q}}_s + [2\omega_A \zeta_A] \dot{\mathbf{q}}_A + [\omega_A^2] \mathbf{q}_A = 0 \quad (14)$$

$$\mathbf{I}\ddot{\mathbf{q}}_s + \Phi_s^T (\mathbf{G}_1^T \{1\}^T + \mathbf{G}_2^T \mathbf{R}_y^T + \mathbf{G}_3^T \mathbf{R}_x^T) \mathbf{M}_A \Phi_A \ddot{\mathbf{q}}_A + [2\omega_s \zeta_s] \dot{\mathbf{q}}_s + [\omega_s^2] \mathbf{q}_s = \mathbf{F}_m \quad (15)$$

The coupling between the host structure and add-on structure is determined by the second term in the above equations. Thus, a coupling coefficient α_{ij} between the i th mode of the add-on structure and the j th mode of the host structure can be defined as

$$\begin{aligned} \alpha_{ij} &= \Phi_{Ai}^T (\mathbf{M}_A \{1\} \mathbf{G}_1 + \mathbf{M}_A \mathbf{R}_y \mathbf{G}_2 + \mathbf{M}_A \mathbf{R}_x \mathbf{G}_3) \Phi_{sj} \\ &= \Phi_{Ai}^T \mathbf{M}_A \{1\} \mathbf{G}_1 \Phi_{sj} + \Phi_{Ai}^T \mathbf{M}_A \mathbf{R}_y \mathbf{G}_2 \Phi_{sj} + \Phi_{Ai}^T \mathbf{M}_A \mathbf{R}_x \mathbf{G}_3 \Phi_{sj} \\ &= \alpha_{i1}^{(1)} \alpha_{j2}^{(1)} + \alpha_{i1}^{(2)} \alpha_{j2}^{(2)} + \alpha_{i1}^{(3)} \alpha_{j2}^{(3)} \end{aligned} \quad (16)$$

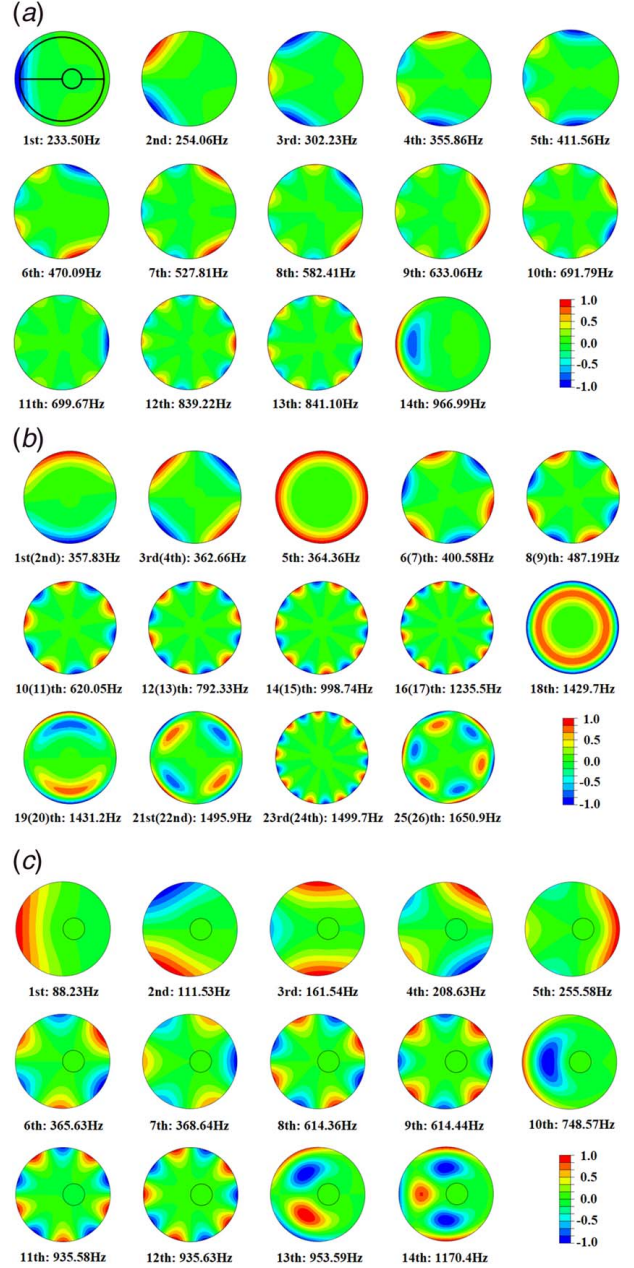


Fig. 7 Modal shapes of the different DVAs: (a) EABH-DVA, (b) SABH-DVA, and (c) EEM-DVA

where

$$\begin{aligned} \alpha_{i1}^{(1)} &= \Phi_{Ai}^T \mathbf{M}_A \{1\}, & \alpha_{i1}^{(2)} &= \Phi_{Ai}^T \mathbf{M}_A \mathbf{R}_y, & \alpha_{i1}^{(3)} &= \Phi_{Ai}^T \mathbf{M}_A \mathbf{R}_x, \\ \alpha_{j2}^{(1)} &= \mathbf{G}_1 \Phi_{sj}, & \alpha_{j2}^{(2)} &= \mathbf{G}_2 \Phi_{sj}, & \alpha_{j2}^{(3)} &= \mathbf{G}_3 \Phi_{sj} \end{aligned} \quad (17)$$

Obviously, $\alpha_{i1}^{(1)}$, $\alpha_{i1}^{(2)}$, and $\alpha_{i1}^{(3)}$ are related to the coupling characteristics of the i th mode shape of add-on structure, Φ_{Ai} , with the

three rigid modes, respectively. In fact, according to the definition of modal participation ratio [43], $\alpha_{i1}^{(k)}$ ($k = 1, 2, 3$) is the modal participation ratio corresponding to the translation in z -axis and rotations with respect to x -axis and y -axis. Equation (17) shows that $\alpha_{j2}^{(1)}$, $\alpha_{j2}^{(2)}$, and $\alpha_{j2}^{(3)}$ depend on the out-of-plane and rotational components of the n th node in the j th mode shape of the host structure, Φ_{sj} . These three components represent the installation position of the absorber, determined by \mathbf{G}_k ($k = 1, 2, 3$). The coupling coefficient is the combined effect of modal participation ratios in the three directions, in relation to the position of installation.

3.2 EABH-DVA in Comparison With the SABH-DVA and EEM-DVA. Dynamics of the three types of add-on devices, namely an asymmetric EABH-DVA, a symmetric ABH-DVA and an eccentric uniform DVA (EEM-DVA) of equal mass, are first investigated and compared. The three devices yield 73, 74, and 50 modes below 5000 Hz, respectively. In addition, an in-plane mode exists in all three structures, which has no effect on the results and is therefore omitted in the subsequent analyses. It is relevant to note that many of the modes appear in pair with the same or very close natural frequency values, and the first 14 modes of the EABH-DVA, including one pair with close frequencies (12th and 13th), are shown in Fig. 7(a). The first 26 modes of the symmetric ABH-DVA structure, including 12 pairs with the same frequencies, and the first 14 modes of EEM-DVA, including three pairs with close frequencies, are shown in Figs. 7(b) and 7(c), respectively. A general observation out of this analysis is the eccentric DVA design that entails an increased number of modes with different natural frequencies, suggesting an enriched dynamics arising from the design. This is expected to be beneficial since previous investigations show that effective ABH-DVA design roots in a well-blended balance between the principles of both dynamic vibration absorbers and waveguide absorbers. Enriched dynamics of the DVA would help increase the chance for creating more effective interaction with the host structure.

As another important attribute of the ABH-based design, the modal damping of the add-on devices, which is vital for achieving effective energy trapping later on, is investigated. DVA effect can effectively suppress the original resonance peak of the host structure, but two new peaks appear at neighboring frequencies. Hence, high damping in the ABH-DVA is necessary to flatten these new peaks. Calculated modal damping factors are shown in Fig. 8. It can be seen that EABH-DVA and SABH-DVA have very similar modal damping ratios, which are all much higher than the EEM-DVA, and this obviously stemming from the ABH effects embedded into the first two devices. But in fact, EABH-DVA has very different dynamic coupling characteristics from SABH-DVA, the asymmetric feature of the EABH-DVA is conducive to better coupling ability with the host structure, which will be discussed in Sec. 3.3. Therefore, the new design is also expected to pump more energy from the host structure to achieve more broadband vibration reduction, especially at high frequencies.

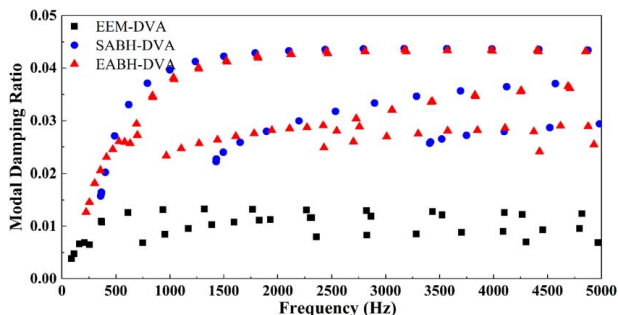


Fig. 8 Damping ratios of the three types of add-on structures

3.3 Coupling Analyses Between the EABH-DVA and the Host Structure. Following the above modal analysis, the modal vectors and the mass matrices for each substructure can be extracted and substituted into Eq. (16) to calculate the modal coupling coefficients between the modes of the host structure and those of each add-on device. The results are shown in Fig. 9. It is obvious that the EABH-DVA has more modes coupled with the host structure than the SABH-DVA. According to Eq. (17), each coupling coefficient consists of three terms and six factors, $\alpha_{i1}^{(1)}$, $\alpha_{i1}^{(2)}$, $\alpha_{i1}^{(3)}$, $\alpha_{j2}^{(1)}$, $\alpha_{j2}^{(2)}$, and $\alpha_{j2}^{(3)}$. The modal coupling occurs if at least one of the three is larger than zero. Note the values of $\alpha_{i1}^{(1)}$, $\alpha_{i1}^{(2)}$, and $\alpha_{i1}^{(3)}$ in turn depend on the modal shapes of the add-on structures.

Figure 9 show that all the first 10 modes of the EABH-DVA are all coupled with the host structure, instead of only three for SABH-DVA (the first, second, and fifth). In order to better understand the underlying mechanism, the continuous version of the coupling coefficient analysis is considered here. Without loss of generality, the function of the i th mode of the add-on structure in a polar coordinate is expressed as $\phi_{Ai}(r, \theta)$. The factor $\alpha_{i1}^{(k)}$ ($k = 1, 2, 3$) in Eq. (17) can be converted into the following form in the continuous space as

$$\alpha_{i1}^{(1)} = \Phi_{Ai}^T \mathbf{M}_A \{1\} = \iint \phi_{Ai}(r, \theta) \rho h(r) r dr d\theta \quad (18)$$

$$\alpha_{i1}^{(2)} = \Phi_{Ai}^T \mathbf{M}_A \mathbf{R}_y = \iint \phi_{Ai}(r, \theta) y \rho h(r) r dr d\theta \quad (19)$$

$$\alpha_{i1}^{(3)} = \Phi_{Ai}^T \mathbf{M}_A \mathbf{R}_x = \iint \phi_{Ai}(r, \theta) x \rho h(r) r dr d\theta \quad (20)$$

In the symmetrical ABH-DVA, r and θ in $\phi_{Ai}(r, \theta)$ are separable and the mode with a radial order m and a circumferential order n is denoted by $RmCn$, whose modal function writes

$$\phi_{Ai}(r, \theta) = \phi_{Anm}(r, \theta) = w_m(r) \cos(n\theta + \theta_0) \quad (21)$$

Substituting Eq. (21) into Eq. (18) gives

$$\begin{aligned} \alpha_{i1}^{(1)} &= \iint w_m(r) \cos(n\theta + \theta_0) \rho h(r) r dr d\theta \\ &= \int w_m(r) \rho h(r) r dr \int \cos(n\theta + \theta_0) \sin \theta d\theta \end{aligned} \quad (22)$$

When $n \geq 1$, $\int_0^{2\pi} \cos(n\theta + \theta_0) \sin \theta d\theta = 0$ so that $\alpha_{i1}^{(1)}$ equals zero, in agreement with the conclusion obtained in Ref. [41] symmetrical DVA.

Substitution of Eq. (21) into Eqs. (19) and (20) gives

$$\begin{aligned} \alpha_{i1}^{(2)} &= \iint w_m(r) \cos(n\theta + \theta_0) \sin \theta \rho h(r) r^2 dr d\theta \\ &= \int w_m(r) \rho h(r) r^2 dr \int \cos(n\theta + \theta_0) \sin \theta d\theta \end{aligned} \quad (23)$$

$$\begin{aligned} \alpha_{i1}^{(3)} &= \iint w_m(r) \cos(n\theta + \theta_0) \cos \theta \rho h(r) r^2 dr d\theta \\ &= \int w_m(r) \rho h(r) r^2 dr \int \cos(n\theta + \theta_0) \cos \theta d\theta \end{aligned} \quad (24)$$

Obviously,

$$\begin{aligned} \int_0^{2\pi} \cos(n\theta + \theta_0) \sin \theta d\theta &= \int_0^{2\pi} \cos(n\theta + \theta_0) \cos \theta d\theta = 0 \\ (n \neq 1) \end{aligned} \quad (25)$$

According to Eqs. (22)–(24), the $RmC0$ mode and the two $RmC1$ modes of the SABH-DVA are coupled with the host structure for

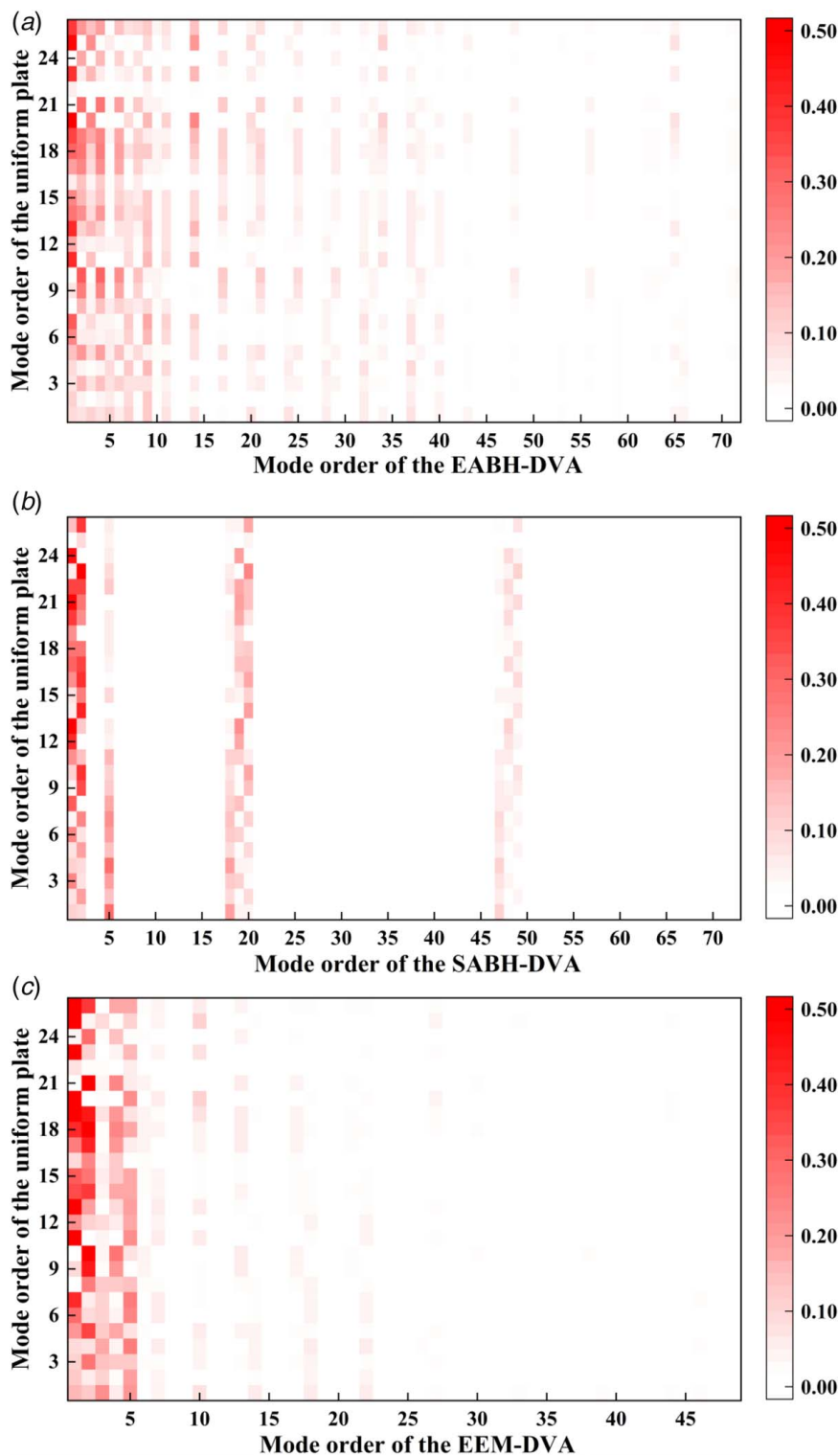


Fig. 9 Modal coupling coefficients between the host structure and the three types of add-on devices below 5000 Hz: (a) EABH-DVA, (b) SABH-DVA, and (c) EEM-DVA

every given m . This is in agreement with Fig. 9(b), where for example, the first, second, and fifth modes are RIC1, RIC1, and RIC0, respectively, similar for some higher-order modes. However, the SABH-DVA has only nine modes coupled with the host structure under 5000 Hz, as shown in Fig. 9(b).

When the axisymmetric of the device is altered in the EABH-DVA, $\phi_{A,i}(r, \theta)$ becomes more complex and the r and θ are not separable anymore. Therefore, theoretically $\alpha_{i1}^{(1)}$, $\alpha_{i1}^{(2)}$, and

$\alpha_{i1}^{(3)}$ in Eqs. (18)–(20) do not become zero for any mode number i . This is true for those i smaller than 10, as shown in Fig. 9(a). However, for $i > 10$, some modes have relatively small coupling coefficient α_{ij} , exemplified by the 12th and 13th modes. The mode shapes of the 12th and 13th are shown in Fig. 7(a). Obviously, their mode shapes are very similar as those of the SABH-DVA, with a large value of circumferential wavenumber n . This explains why α_{ij} are small. The results of modal analysis

show that these types of quasi-axisymmetric modes become denser in the high frequency range.

The coupling strength of the EEM-DVA with the host structure is shown in Fig. 9(c). It is obvious that EEM-DVA has more modes coupled with the host structure than the SABH-DVA does, but less than the EABH-DVA. As an example, the eighth and the ninth modes of the EEM-DVA, which are not coupled with host structure, are the quasi-axisymmetric modes shown in Fig. 7(c). The quasi-axisymmetric modes appear at a lower frequency in the EEM-DVA than in the EABH-DVA. The EEM-DVA also has more quasi-axisymmetric modes than the EABH-DVA.

4 Vibration Reduction with the EABH-DVA

4.1 Numerical Results. The mobility of the plate alone which of the combined system with EABH-DVA or with SABH-DVA is shown in Fig. 10(a). The modal damping ratios corresponding to all the visible resonance peaks in the combined systems with EABH-DVA and SABH-DVA are also shown in Fig. 10(b). Compared with SABH-DVA, the EABH-DVA yields more significant peak reductions in the plate vibration, in almost the entire frequency range being considered here. The enhanced damping effect of the EABH-DVA as compared with the SABH-DVA can be attributed to a more effective coupling between the two sub-systems, thus promoting the dynamics of the device and facilitating more effective energy transfer with the host plate, as shown in Fig. 9.

A closer examination of the changes in the vibration response of the host plate allows a better understanding of the physical process incurred in the system. While the second resonant modal response of the host plate (345.41 Hz) is significantly reduced by both the EABH-DVA and SABH-DVA, the first mode (267.41 Hz) can only be coped with by the EABH-DVA. With the EABH-DVA, typical DVA phenomenon in terms of dynamic interaction (between the second mode, 254.06 Hz, of the EABH-DVA and the first mode of the host structure) can be seen, since the original peak is split into two. Similar phenomena can also be observed for some resonances between 1000 Hz and 3000 Hz. Another typical phenomenon is related to damping, arising from the waveguide effects of the ABH absorbers. In fact, the damping effects of both the EABH-DVA and the SABH-DVA at the fifth mode of the host structure (760.93 Hz) are very close, but the control performance of the EABH-DVA is much better than that of the SABH-DVA. This phenomenon again can be explained from the coupling perspective. As the closest mode to the fifth mode of the plate, the 11th EABH-DVA mode at about 699.67 Hz is weakly coupled with the fifth mode of the host structure (with a coupling coefficient of 0.0203). In comparison, the 12th mode of the SABH-DVA at 792.33 Hz is the closest to the fifth mode of the host plate, but it is not coupled at all with host structure. Therefore, the damping effect achieved at the fifth mode of the host structure is mainly from the first three coupled modes (first, second, and fifth) of the SABH-DVA. The lower-order modes would contribute to the damping of all the coupled modes of the host structure without

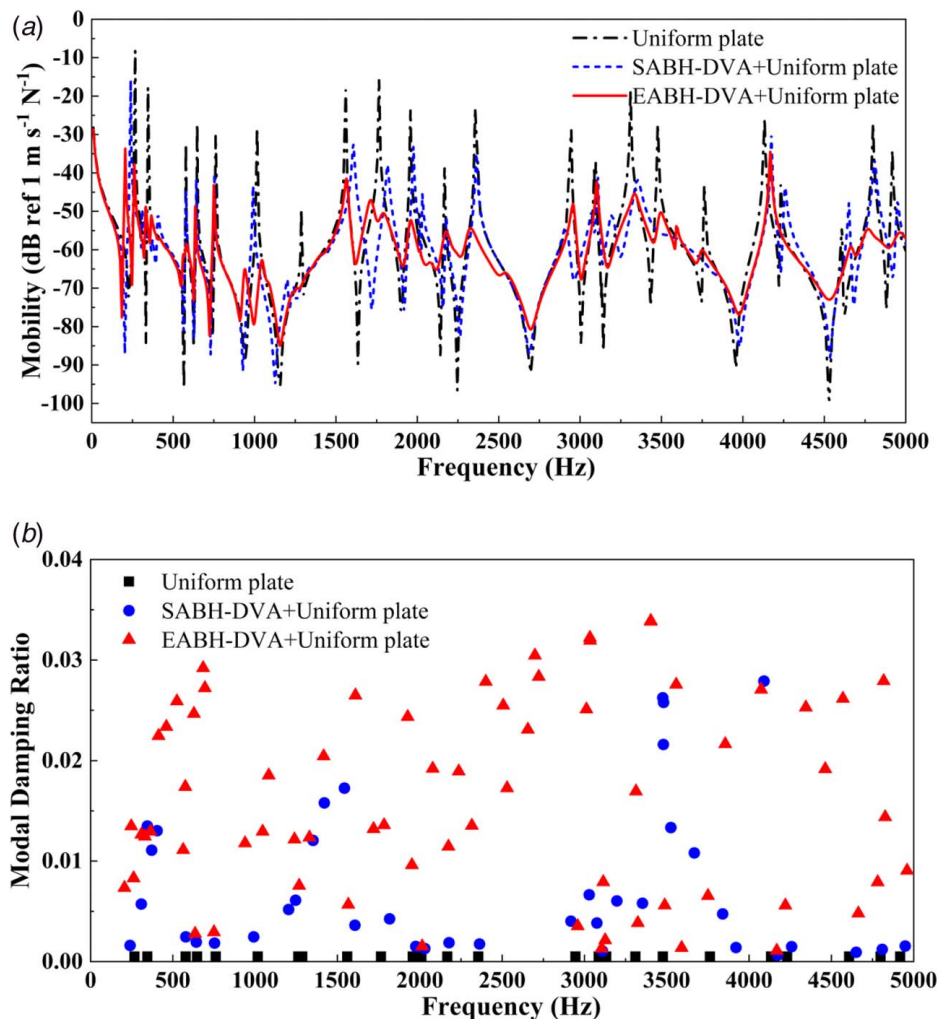


Fig. 10 Comparisons of the driving point mobility and modal damping ratio of the host plate with different add-on ABH-DVAs: (a) driving point mobility and (b) modal damping ratio

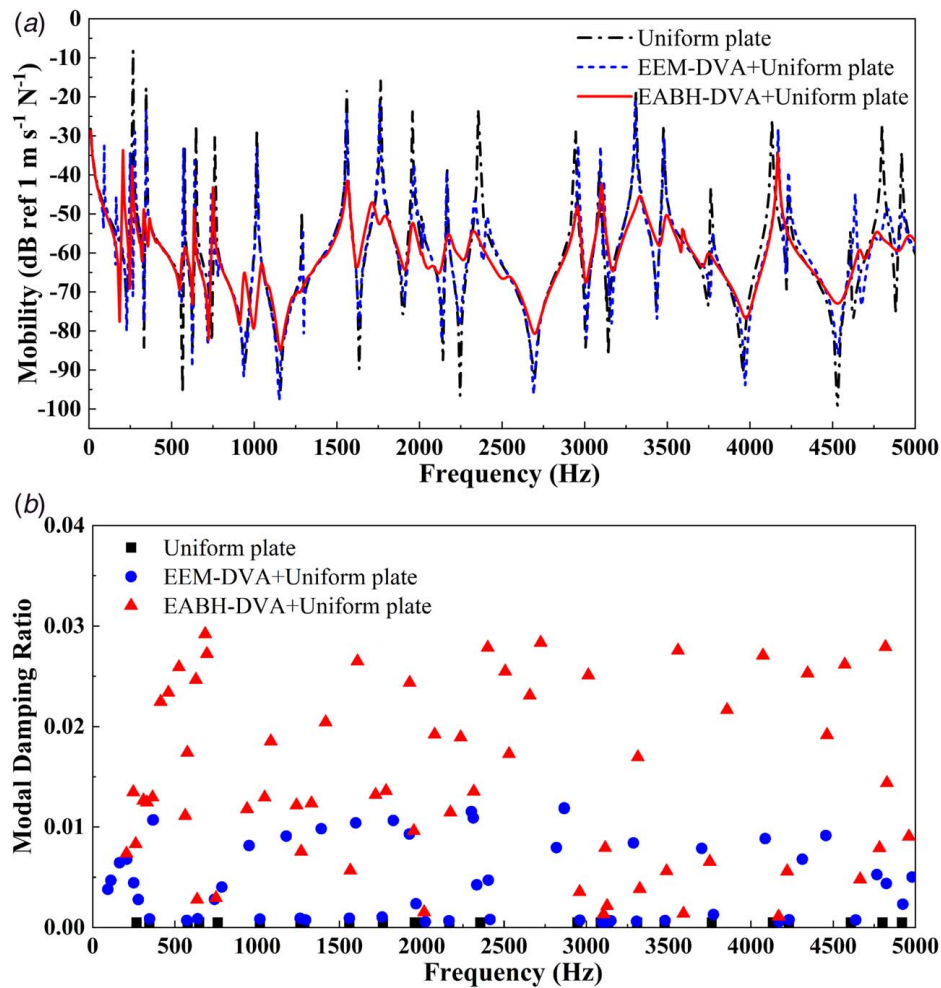


Fig. 11 Comparisons of the driving point mobility and modal damping ratio of the host plate with different eccentric DVAs: (a) driving point mobility and (b) modal damping ratio

dominant dynamic interaction effect, the mechanism of which was discussed in the former study [41]. Although SABH-DVA and EABH-DVA have very similar modal damping ratios (Fig. 8), as demonstrated earlier in Fig. 9, the vast majority of the SABH-DVA cannot be coupled with the host structure due to its symmetrical design. As a result, these uncoupled modes (as well as their damping effects) cannot play out to affect the host structure. Therefore, the remarkable vibration suppression capability of the proposed EABH-DVA is indeed attributed to the enriched structural coupling and the enhanced modal damping, arising from the eccentric and circumferentially graded ABH design.

To further confirm the role that ABH plays in the entire physical process, Fig. 11 compares the cases using EABH-DVA with the one using EEM-DVA (uniform disk) in terms of the driving point mobility of the host plate (Fig. 11(a)) and modal damping ratios of the combined structure (Fig. 11(b)). Comparison shows that, although performance might be close for some particular resonant peaks in both cases, EABH-DVA generally outperforms the EEM-DVA as expected. It is also noteworthy that, owing to its eccentric nature, although the EEM-DVA has better coupling ability than the SABH-DVA at low frequencies, the broadband effect is still limited due to the low damping of the EEM-DVA in the absence of ABH effect. For example, the peak split of first mode of the host structure is obvious DVA effect. Meanwhile, the number of quasi-axisymmetric modes in the EEM-DVA is also noticed to be larger than that in EABH-DVA in the high frequency range, as shown in Fig. 7(c). Similarly, they also have smaller damping ratios compared with EABH-DVA modes, for the same reason mentioned above. To sum up, due to its higher

modal damping ratio and denser and strongly coupled modes, the EABH-DVA yields better broadband damping in the combined system than the SABH-DVA and EEM-DVA do. This adds up with the enhanced dynamic interaction effects for specific mode pairs, to achieve an overall broadband vibration reduction in the host structure, as numerically demonstrated up to now.

In summary, enriching structural coupling and enhancing modal damping are two vital parameters to be considered. The eccentric and circumferentially graded ABH design of the EABH-DVA allows this to happen. The proposed design also allows the two fundamental mechanisms underpinning the effective operation of vibration absorbers (dynamic interaction and energy trapping) to be fully embraced and play out. To better its difference with other designs, a qualitative comparison is summarized in Table 3.

4.2 Effects of the Eccentricity. As an important design parameter, the effects of the eccentricity in the EABH-DVA are

Table 3 Comparison of dynamic coupling and damping characteristics of different DVAs

Model	Dynamic coupling strength	Damping	Control performance
EEM-DVA	High	Low	Fair
SABH-DVA	Fair	High	Good
EABH-DVA	High	High	Excellent

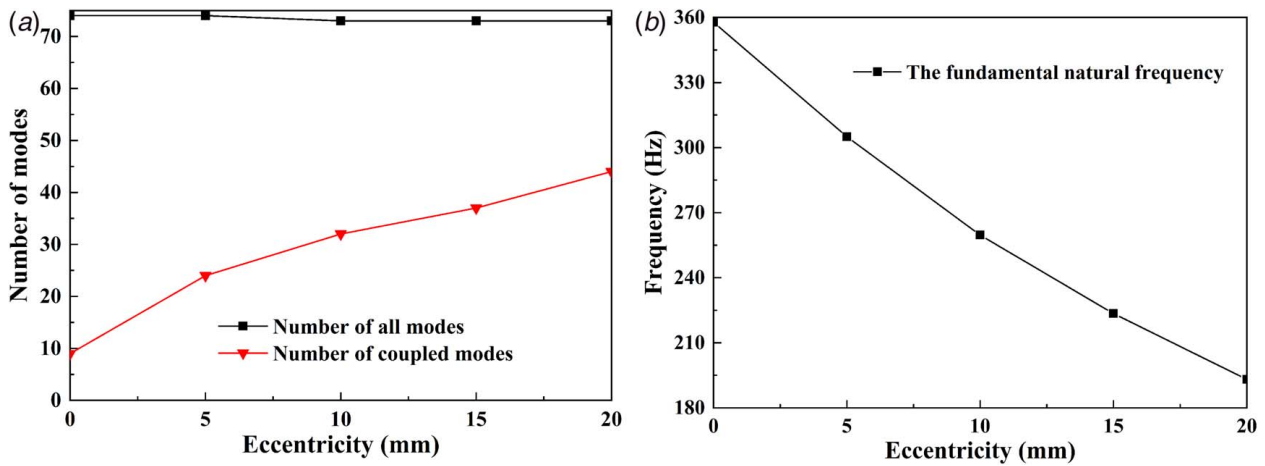


Fig. 12 Variation of the number of modes and the fundamental natural frequency of EABH-DVA with eccentricity e below 5000 Hz: (a) number of modes and (b) the fundamental natural frequency of EABH-DVA

examined. The dynamics of the EABH-DVA in terms of number of modes and natural frequencies for different eccentricity e , varying from 0 to 20 mm at a 5 mm intervals are analyzed. The number of modes up to 5000 Hz and the fundamental natural frequency of the ABH device with different e values are shown in Fig. 12. As can be seen from Fig. 12(a), with the increase of eccentricity, the total number of modes under 5000 Hz basically does not change, but the number of modes coupled with the host structure gradually increases. Meanwhile, as e increases, the fundamental natural frequency decreases as shown in Fig. 12(b), which also increases the number of low-frequency modes that could be coupled to the host structure. This also confirms that the proposed EABH-DVA does exhibit richer dynamics than SABH-DVA ($e = 0$). By the same token, this also increases the chance of creating better frequency matching with the host structure and more effective and energetic energy exchanges. While the former is essential to achieve the dynamic absorber effects, the latter is indispensable in waveguide absorbers. These two vibration reduction principles are fully played out with the eccentric design of the ABH absorbers. Therefore, it can be concluded that the increase of eccentricity is conducive to vibration suppression. The larger the eccentricity is, the larger the number of coupled modes.

5 Experimental Verifications

Experiments were conducted to provide a qualitative verification of the numerically predicted broadband vibration suppression phenomena and typical vibration control effects. The EABH disk and other disks used for comparisons were made of aluminum and were manufactured through computer numerical control (CNC)

milling. The host plate under control was also made of aluminum. The damping layer was a ring of butyl rubber with a width of 30 mm. The sizes of all test samples were the same as the ones used in the above simulations. Free boundary condition was realized by suspending the plate using two elastic strings attached to a rigid frame. The add-on ABH devices were fixed onto the host plate using a standard 5 mm screw. Figure 13 shows the experimental setup. An electromagnetic shaker (B&K 4809), driven by a power amplifier (B&K 2718), was used to generate a periodic chirp force from 10 Hz to 5000 Hz to excite the plate at (100, 50) mm. The response measurement was performed using a Polytec™ Laser Scanning Vibrometer (PSV 500).

The driving mobility curves and the mean velocities of the host plate without and with different DVAs were measured up to 5000 Hz, and the results are compared in Fig. 14. It can be observed that among all test cases, the EABH-DVA generally leads to the best control performance, in terms of both resonant peak attenuation and broadband vibration reduction, except for some particular frequencies such as 3145 Hz and 4170 Hz. The deficiency at these specific frequencies is due to the specific installation location of the DVAs, which can be alleviated either by changing the location or increasing the number of DVAs. Having said that, the observed vibration reduction trends as well as the relative levels relating to each type of DVAs are basically consistent with numerical predictions. The superior vibration reduction performance of the EABH-DVA over other DVAs, within the broad frequency range as well as at some critical frequencies such as 264 Hz, 780 Hz, 1560 Hz, 1993 Hz, 2193 Hz, and 3000 Hz, are particularly noteworthy. As demonstrated in numerical simulations, this is owing to the eccentric ABH-enabled features of the EABH-DVA (rich dynamics, large coupling coefficient and high damping), which enhance

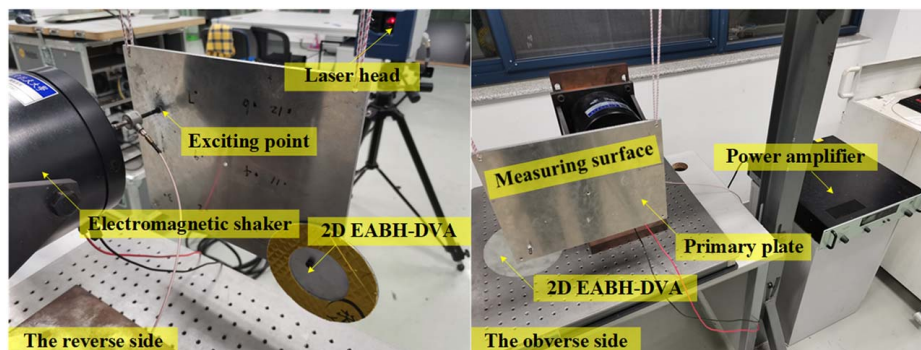


Fig. 13 Experimental test setup

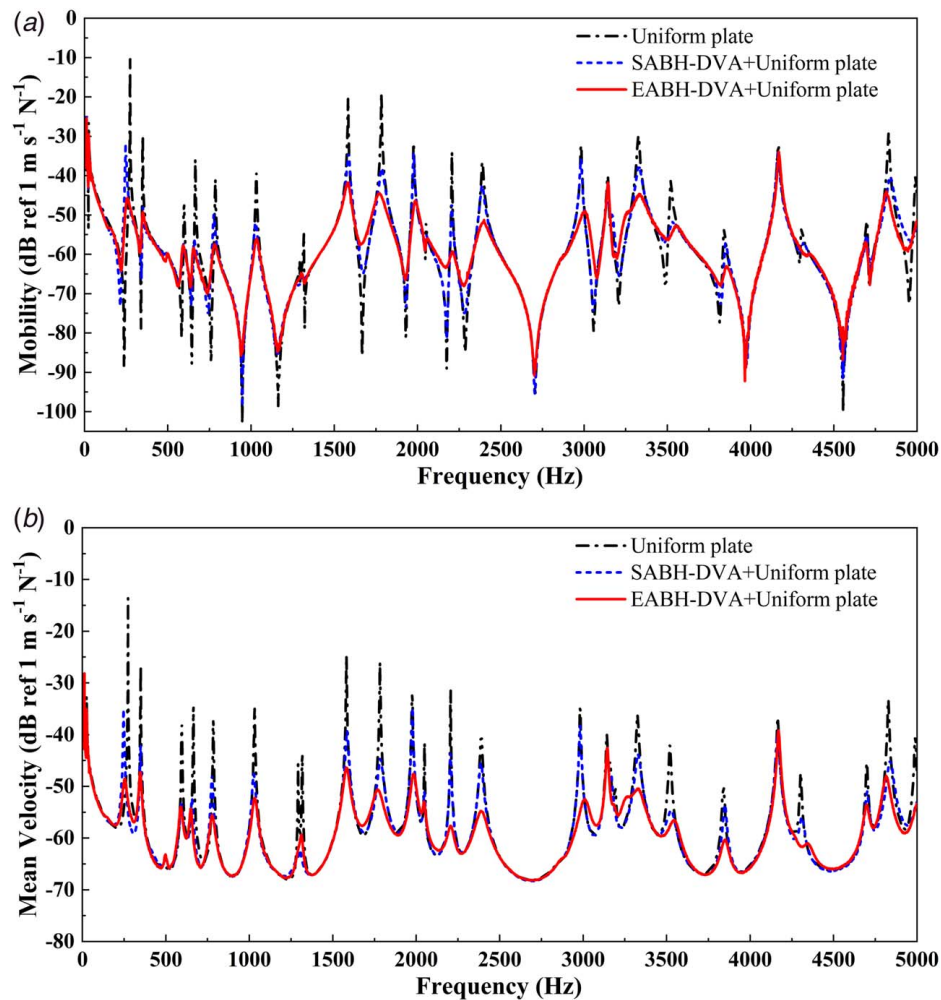


Fig. 14 Experimentally measured vibration responses of the host plate without and with different DVAs: (a) driving point mobility and (b) mean velocity of plate surface

its coupling with the host plate. This, along with the aggregated damping enhancement on most of structural modes, collectively contributes to a broadband vibration reduction of the system.

6 Conclusions

This paper proposes an eccentric ABH-based circular DVA, to be surface-mounted onto a vibrating structure for its vibration reduction. The proposed configuration preserves the ABH profile in the radial direction alongside a continuous variation along circumferential direction. This leads to a compact and light-weight vibration reduction device with enriched ABH features and enhanced coupling with a host structure without the any tedious tuning procedure which is usually needed in conventional DVAs. Theoretical and numerical analyses are conducted to compute the coupling coefficient between the ABH-DVAs and the host structure, which is a vital parameter to guide the system design. The superiority of the proposed EABH-DVA over other DVA designs for the same given mass is demonstrated both numerically and experimentally. The proposed EABH-DVA is shown to be able to entail a significant and broadband vibration reduction of a host structure, exemplified by the attenuation of most resonant peaks in a host plate and an overall reduction of the vibration level over the entire structure. The enriched structural coupling and the enhanced modal damping, arising from the eccentric and circumferentially graded ABH design of the EABH-DVA, are shown to be the origin of such performance. The proposed design allows the two fundamental

mechanisms underpinning the effective operation of vibration absorbers (dynamic interaction and energy trapping) to be fully embraced and play out: an enriched dynamic of the DVA increases the chance for creating more effective interaction with the host structure, while the embedded ABH features enable more effective wave trapping and dissipation of energy pumped from the host structure.

This study might offer new impetus to the exploration of the ABH-based technology for practical engineering applications, an area which is still much needed in the general arena of ABH research.

Acknowledgment

This work is partially supported by the National Natural Science Foundation of China (Nos. 52022039, 51775267, and 52105107), the Rapid Support Projects (No. 80910010102), the Research Fund of State Key Laboratory of Mechanics and Control of Mechanical Structures (Nanjing University of Aeronautics and astronautics, No. MCMS-I-0521G03 & MCMS-E-0521Y01), and the Priority Academic Program Development of Jiangsu Higher Education Institutions.

Conflict of Interest

There are no conflicts of interest.

Data Availability Statement

The authors attest that all data for this study are included in the paper.

References

- [1] Hill, S. G., and Snyder, S. D., 2002, "Design of an Adaptive Vibration Absorber to Reduce Electrical Transformer Structural Vibration," *ASME J. Vib. Acoust.*, **124**(4), pp. 606–611.
- [2] Lv, H., and Leamy, M. J., 2021, "Damping Frame Vibrations Using Anechoic Stubs: Analysis Using an Exact Wave-Based Approach," *ASME J. Vib. Acoust.*, **143**(5), p. 051012.
- [3] Krylov, V. V., and Tilman, F. J. B. S., 2004, "Acoustic 'Black Holes' for Flexural Waves as Effective Vibration Dampers," *J. Sound Vib.*, **274**(3–5), pp. 605–619.
- [4] Krylov, V. V., 2004, "New Type of Vibration Dampers Utilising the Effect of Acoustic 'Black Holes'," *Acta Acust. Acust.*, **90**(5), pp. 830–837.
- [5] Georgiev, V. B., Cuenca, J., Gautier, F., Simon, L., and Krylov, V. V., 2011, "Damping of Structural Vibrations in Beams and Elliptical Plates Using the Acoustic Black Hole Effect," *J. Sound Vib.*, **330**(11), pp. 2497–2508.
- [6] Cheer, J., Hook, K., and Daley, S., 2021, "Active Feedforward Control of Flexural Waves in an Acoustic Black Hole Terminated Beam," *Smart Mater. Struct.*, **30**(3), p. 035003.
- [7] Huang, W., Ji, H., Qiu, J., and Cheng, L., 2016, "Wave Energy Focalization in a Plate With Imperfect Two-Dimensional Acoustic Black Hole Indentation," *ASME J. Vib. Acoust.*, **138**(6), p. 061004.
- [8] Leng, J., Romero-García, V., Pelat, A., Picó, R., Groby, J.-P., and Gautier, F., 2020, "Interpretation of the Acoustic Black Hole Effect Based on the Concept of Critical Coupling," *J. Sound Vib.*, **471**, p. 115199.
- [9] Krylov, V. V., and Winward, R. E. T. B., 2007, "Experimental Investigation of the Acoustic Black Hole Effect for Flexural Waves in Tapered Plates," *J. Sound Vib.*, **300**(1–2), pp. 43–49.
- [10] Kralovic, V., and Krylov, V. V., 2007, "Damping of Flexural Vibrations in Tapered Rods of Power-Law Profile: Experimental Studies," *Proc. Inst. Acoust.*, **29**(5), pp. 66–73.
- [11] Bowyer, E. P., O'Boy, D. J., Krylov, V. V., and Gautier, F., 2013, "Experimental Investigation of Damping Flexural Vibrations in Plates Containing Tapered Indentations of Power-Law Profile," *Applied Acoustics*, **74**(4), pp. 553–560.
- [12] Feurtado, P. A., and Conlon, S. C., 2016, "An Experimental Investigation of Acoustic Black Hole Dynamics at Low, Mid, and High Frequencies," *ASME J. Vib. Acoust.*, **138**(6), p. 061002.
- [13] Tang, L., Cheng, L., Ji, H., and Qiu, J., 2016, "Characterization of Acoustic Black Hole Effect Using a One-Dimensional Fully-Coupled and Wavelet-Decomposed Semi-Analytical Model," *J. Sound Vib.*, **374**, pp. 172–184.
- [14] Bayod, J. J., 2011, "Experimental Study of Vibration Damping in a Modified Elastic Wedge of Power-Law Profile," *ASME J. Vib. Acoust.*, **133**(6), p. 061003.
- [15] Conlon, S. C., Fahline, J. B., and Semperlotti, F., 2015, "Numerical Analysis of the Vibroacoustic Properties of Plates with Embedded Grids of Acoustic Black Holes," *J. Acoust. Soc. Am.*, **137**(1), pp. 447–457.
- [16] Gao, N., Wei, Z., Hou, H., and Krushynska, A. O., 2019, "Design and Experimental Investigation of V-Folded Beams with Acoustic Black Hole Indentations," *J. Acoust. Soc. Am.*, **145**(1), pp. EL79–EL83.
- [17] Deng, J., Zheng, L., Zeng, P., Zuo, Y., and Guasch, O., 2019, "Passive Constrained Viscoelastic Layers to Improve the Efficiency of Truncated Acoustic Black Holes in Beams," *Mech. Syst. Signal Process.*, **118**, pp. 461–476.
- [18] Shepherd, M. R., McCormick, C. A., Conlon, S. C., and Feurtado, P. A., 2017, "Modeling and Optimization of Acoustic Black Hole Vibration Absorbers," *J. Acoust. Soc. Am.*, **141**(5), pp. 4034–4034.
- [19] McCormick, C. A., and Shepherd, M. R., 2020, "Design Optimization and Performance Comparison of Three Styles of One-Dimensional Acoustic Black Hole Vibration Absorbers," *J. Sound Vib.*, **470**, p. 115164.
- [20] Ma, L., Dong, H.-W., and Cheng, L., 2020, "An Alternative and Optimized Thickness Profile of an Acoustic Black Hole Plate," *J. Sound Vib.*, **486**, p. 115619.
- [21] Bowyer, E. P., and Krylov, V. V., 2014, "Experimental Investigation of Damping Flexural Vibrations in Glass Fibre Composite Plates Containing One- and Two-Dimensional Acoustic Black Holes," *Compos. Struct.*, **107**, pp. 406–415.
- [22] Bowyer, E. P., and Krylov, V. V., 2015, "Experimental Study of Sound Radiation by Plates Containing Circular Indentations of Power-Law Profile," *Appl. Acoust.*, **88**, pp. 30–37.
- [23] Bowyer, E. P., and Krylov, V. V., 2015, "A Review of Experimental Investigations Into the Acoustic Black Hole Effect and Its Applications for Reduction of Flexural Vibrations and Structure-Borne Sound," *Inter-Noise*, San Francisco, Aug. 9–12. <https://www.researchgate.net/publication/282186765>
- [24] Zhao, L., Conlon, S. C., and Semperlotti, F., 2014, "Broadband Energy Harvesting Using Acoustic Black Hole Structural Tailoring," *Smart Mater. Struct.*, **23**(6), p. 065021.
- [25] Zhao, L., 2016, "Passive Vibration Control Based on Embedded Acoustic Black Holes," *ASME J. Vib. Acoust.*, **138**(4), p. 041002.
- [26] Pelat, A., Gautier, F., Conlon, S. C., and Semperlotti, F., 2020, "The Acoustic Black Hole: A Review of Theory and Applications," *J. Sound Vib.*, **476**, p. 115316.
- [27] Zhao, C., and Prasad, M. G., 2019, "Acoustic Black Holes in Structural Design for Vibration and Noise Control," *Acoustics*, **1**(1), pp. 220–251.
- [28] Frahm, H., 1909, "Device for Damping Vibrations of Bodies," U. S. Patent No. 989958.
- [29] Ormondroyd, J., and Den Hartog, J. P., 1928, "The Theory of Dynamic Vibration Absorber," *ASME J. Appl. Mech.*, **50**(7), pp. 9–22.
- [30] Asami, T., and Nishihara, O., 1999, "Analytical and Experimental Evaluation of an Air Damped Dynamic Vibration Absorber: Design Optimizations of the Three-Element Type Model," *ASME J. Vib. Acoust.*, **121**(3), pp. 334–342.
- [31] Asami, T., and Nishihara, O., 2002, "H2 Optimization of the Three-Element Type Dynamic Vibration Absorbers," *ASME J. Vib. Acoust.*, **124**(4), pp. 583–592.
- [32] Ren, M. Z., 2001, "A Variant Design of the Dynamic Vibration Absorber," *J. Sound Vib.*, **245**(4), pp. 762–770.
- [33] Ozer, M., and Royston, T., 2005, "Extending Den Hartog's Vibration Absorber Technique to Multi-Degree-of-Freedom Systems," *ASME J. Vib. Acoust.*, **127**(4), pp. 341–350.
- [34] Zuo, L., and Nayfeh, S. A., 2004, "Minimax Optimization of Multi-Degree-of-Freedom Tuned-Mass Dampers," *J. Sound Vib.*, **272**(3), pp. 893–908.
- [35] Zuo, L., and Nayfeh, S. A., 2006, "The Two-Degree-of-Freedom Tuned-Mass Damper for Suppression of Single-Mode Vibration Under Random and Harmonic Excitation," *ASME J. Vib. Acoust.*, **128**(1), pp. 56–65.
- [36] Jacquot, R. G., and Foster, J. E., 1977, "Optimal Cantilever Dynamic Vibration Absorbers," *J. Ind. Eng. Int.*, **99**(1), pp. 138–141.
- [37] Snowdon, J. C., Wolfe, A. A., and Kerlin, R. L., 1984, "The Cruciform Dynamic Vibration Absorber," *J. Acoust. Soc. Am.*, **75**(6), pp. 1792–1799.
- [38] Zuo, L., and Nayfeh, S., 2005, "Optimization of the Individual Stiffness and Damping Parameters in Multiple-Tuned-Mass-Damper Systems," *ASME J. Vib. Acoust.*, **127**(1), pp. 77–83.
- [39] Giaralis, A., and Taflanidis, A. A., 2018, "Optimal Tuned Mass-Damper-Inerter (TMDI) Design for Seismically Excited MDOF Structures with Model Uncertainties Based on Reliability Criteria," *Struct. Control Health Monit.*, **25**(2), p. e2082.
- [40] Zhou, T., and Cheng, L., 2018, "A Resonant Beam Damper Tailored with Acoustic Black Hole Features for Broadband Vibration Reduction," *J. Sound Vib.*, **430**, pp. 174–184.
- [41] Ji, H., Wang, N., Zhang, C., Wang, X., Cheng, L., and Qiu, J., 2021, "A Vibration Absorber Based on Two-Dimensional Acoustic Black Holes," *J. Sound Vib.*, **500**, p. 116024.
- [42] Zhou, T., and Cheng, L., 2022, "Planar Swirl-Shaped Acoustic Black Hole Absorbers for Multi-Directional Vibration Suppression," *J. Sound Vib.*, **516**, p. 116500.
- [43] Wijk, J., 2008, *Spacecraft Structures*, Springer-Verlag, Heidelberg/Berlin, Germany.